ALCHEMY Jurnal Penelitian Kimia

Official Website: https://jurnal.uns.ac.id/alchemy

ISSN 1412-4092
EISSN 2443-4183

An rGO-decorated TiO_2-Fe_2O_3 Ternary Composite for Photocatalysis of Tetracycline Under Visible Light Irradiation

Anthoni Batahan Aritonang[a*], Hafsoh Tri Mustika Rahimi[a], Muhamad Agus Wibowo[a], Warsidah Warsidah[b]

[a]*Department of Chemistry, Faculty of Mathematics and Natural Sciences, Tanjungpura University*
[b]*Department of Oceanography, Faculty of Mathematics and Natural Sciences, Tanjungpura University*
Jalan Prof. Dr. H. Hadari Nawawi No 1, Bansir Laut, Pontianak Tenggara, Pontianak, Kalimantan Barat 78124, Indonesia

[*]*Corresponding author: anthoni.b.aritonang@chemistry.untan.ac.id*

DOI: 10.20961/alchemy.22.2.123560.452-462

Received 13 July 2026, Revised 5 September 2026, Accepted 11 September 2026, Published 30 September 2026

Keywords:

degradation; photocatalytic; tetracycline; TiO_2/Fe_2O_3/rGO; visible light.

ABSTRACT. Tetracycline (TC) antibiotic residues entering water bodies pose a global health threat, necessitating technology to reduce their concentration. Photocatalysis of rGO-modified TiO_2/Fe_2O_3 composites can degrade TC into simple molecules that are harmless to the environment. In this study, an rGO-decorated TiO_2/Fe_2O_3 composite was successfully synthesized using a combined green synthesis and hydrothermal method. The green-synthesized TiO_2 exhibited a band gap of 3.26 eV. Incorporating Fe_2O_3 into the TiO_2 matrix reduced the band gap to 2.97 eV and demonstrated good photocatalytic activity for the degradation of 30 ppm tetracycline (TC) under visible light irradiation for 120 minutes, achieving a degradation efficiency of 54%. The addition of rGO at weight ratios of 1%, 2%, and 3% to the TiO_2/Fe_2O_3 matrix formed TiO_2/Fe_2O_3 /rGO composites designated as TF1, TF2, and TF3 with band gaps of 2.92, 2.82, and 2.94 eV, respectively. The optimal rGO-to-TiO_2/Fe_2O_3 weight ratio was 2% (TF2), yielding the highest TC degradation efficiency of 72%. This enhanced photocatalytic activity for TC degradation stems from the synergistic contribution between the TiO_2/Fe_2O_3 heterojunction composite and rGO, facilitated by charge-pair separation through charge transfer from the TiO_2/Fe_2O_3 to the rGO surface.

INTRODUCTION

The persistent presence of tetracycline (TC) in aquatic systems can increase the risk of bacterial resistance spreading, posing a threat to global health (Mohammadi *et al.*, 2023; Xu *et al.*, 2021). This is because approximately 75% of antibiotics consumed are not fully absorbed by the body; consequently, they are typically excreted in active forms that can damage environmental ecosystems (Elmund *et al.*, 1971; Xu *et al.*, 2021). Therefore, TC needs to be degraded into simpler, less harmful molecules, a process that can be achieved using titanium dioxide (TiO_2)-based photocatalysis (Silerio-Vázquez *et al.*, 2024). Under UV irradiation, the TiO_2 photocatalytic mechanism generates hydroxyl radicals (HO•), which can oxidize organic substrates and inhibit pathogenic bacteria (Rathi *et al.*, 2023).

From a chemical perspective, TiO_2 can be synthesized via a green method that uses a biomass extract as both a reducing and stabilizing agent for nanoparticle formation (Aritonang *et al.*, 2025; Mohamed *et al.*, 2019). In our recent study, a TiO_2 photocatalyst was synthesized using seaweed extract (*Sargassum sp.*). The resulting TiO_2 exhibited photocatalytic activity under UV irradiation, achieving up to 79% degradation of methylene blue over 180 minutes. However, a TiO_2 has a wide band gap energy (3.0 – 3.2 eV) and is only able to absorb UV light, thus limiting its applications (Aritonang *et al.*, 2018). Consequently, the surface optical properties of TiO_2 require modification to enable the utilization of the visible light spectrum. Forming TiO_2-based composites is an effective approach to modifying the surface electronic structure, thereby enhancing photocatalytic activity.

Our previous research on combining TiO_2 with the semiconductor Fe_2O_3 (band gap of 2.2 eV) has shown that this combination expands the absorption range in the visible spectrum (Rashid *et al.*, 2025). However, the

Cite this as: Aritonang, A. B., Rahimi, H. T. M., Wibowo, M. A., and Warsidah, W. (2026). An rGO-decorated TiO_2-Fe_2O_3 Ternary Composite for Photocatalysis of Tetracycline Under Visible Light Irradiation. *ALCHEMY Jurnal Penelitian Kimia*, 22(2), 452-462. doi: https://dx.doi.org/10.20961/alchemy.22.2.123560.452-462.

Copyright © 2026, Universitas Sebelas Maret, ISSN 1412-4092, e ISSN 2443-4183

photocatalytic efficiency remains relatively low due to the high recombination of electron-hole pairs (Mohammadi *et al*., 2023). Reduced graphene oxide (rGO) is a two-dimensional (2D) carbon-based material composed of sheets of sp2-hybridized carbon atoms arranged in a hexagonal, honeycomb-like lattice, characterized by high conductivity and stability (Padmanabhan et al., 2021). With a relatively small bandgap (1.00 – 1.69 eV), rGO shows great potential for forming composites with semiconductors such as TiO_2 for use as a photocatalytic material, as it provides surface active sites and facilitates charge transfer (Hidayati *et al*., 2021; Utami *et al*., 2024). These enhanced properties make rGO an excellent candidate for compositing with other semiconductor materials, as it improves charge transfer and suppresses electron-hole pair recombination, thereby increasing photocatalytic efficiency (Rashid *et al*., 2025). Botsa (2025) reported a ternary nanocomposite composed of reduced graphene oxide (rGO), Fe_2O_3, and TiO_2.

The extensive, net-like surface of rGO facilitates the transfer of photoelectrons to external active sites, promoting electron-hole separation and suppressing recombination, thereby enhancing the efficiency of nitrobenzene degradation (Botsa, 2025). This increased activity is attributed to effective charge separation resulting from the addition of rGO, as well as the synergistic interaction between TiO_2 and Fe_2O_3 (Jo and Selvam, 2015; Zheng *et al*., 2023). However, the influence of rGO concentration on the characteristics and performance of the TiO_2/Fe_2O_3/rGO heterostructure composite has not yet been discussed in detail.

This study investigates the effect of varying rGO concentrations (1, 2, and 3%) on TiO_2/Fe_2O_3 composites, designated as $TiO_2/Fe_2O_3/rGO_x$ (where x = 1, 2, or 3%). The resulting composites were characterized using appropriate methods to determine their crystal phase structure, functional groups, and band gap energy. Subsequently, the photocatalytic performance of the $TiO_2/Fe_2O_3/rGO_x$ composites was evaluated based on the degradation of a TC solution (30 ppm) under visible light irradiation.

RESEARCH METHODS

The equipment and instrumentation used in this study consisted of a Fourier transform infrared (FTIR) spectrometer (Shimadzu IRPrestige-21), a UV-Vis spectrophotometer (Thermo Scientific Orion AquaMate 8100 (AQ8100)), a Diffuse Reflectance UV-Vis (DRS UV-Vis) spectrophotometer (PerkinElmer LAMBDA 365), a Surface Area Analyzer (SAA; Quantachrome Novatouch Lx4), an X-Ray Diffractometer (XRD; PW3040/60 PANalytical), and a Particle Size Analyzer (PSA; Horiba SZ-100-Z), as well as supporting equipment such as an ultrasonic cleaning machine (JOANLAB UC20D) and a photocatalytic reactor unit.

The materials used included titanium tetraisopropoxide (97%, Sigma-Aldrich), iron(III) nitrate nonahydrate (Merck, p.a. 99.99%), potassium permanganate (Merck), graphite powder (Merck), hydrochloric acid (37%), sulfuric acid (98%), ethanol (p.a. 98%, SmartLab), ethylene glycol (1,2-ethanediol, pro-analysis grade, Rofa), and tetracycline hydrochloride (Sigma-Aldrich); brown seaweed (*Sargassum sp*.) was collected from the coast of Lemukutan Island, Karimunting Village, Sungai Raya, West Kalimantan. Chemicals obtained from the market were used directly without further purification.

Extraction of *Sargassum sp*.

Fresh brown seaweed (*Sargassum sp.*) was extracted using the maceration method, as reported by Septiyanti et al. (2019). First, fresh Sargassum sp. was washed with running water, dried in a vacuum dryer at 40 °C, and then ground in a blender into a powder. A total of 600 g of Sargassum sp. powder was prepared in a container, then 1,500 mL of ethanol (96%) was added, and the mixture was soaked 3 times, 24 hours each, until a brownish-yellow extract mixture was formed. Next, the extract was filtered and concentrated on a rotary evaporator at 40 °C until a thick, greenish-brown extract was obtained, ready for TiO_2/Fe_2O_3 synthesis.

Green Synthesis of TiO_2

TiO_2 was synthesized using a green method based on the procedure described by Rashid *et al*. (2025), with slight modifications. First, a Ti(OH)n sol was prepared from a mixture of Solution A, consisting of 2 mL of acetic acid, 2 mL of demineralized water, and 26.5 mL of ethanol, and Solution B, consisting of 26.5 mL of ethanol and 7.5 mL of titanium tetraisopropoxide (TTIP). Solution A was gradually added to Solution B while stirring until the mixture became homogeneous. Once the addition of Solution A was complete, the mixture was heated to 55 °C. Then, 0.25 g of the extract was added to the mixture under constant stirring for 2 hours, yielding a pale yellow TiO_2 sol. A portion of the TiO_2 sol was stored in a dark bottle for subsequent stages, while another portion was

Copyright © 2026, Universitas Sebelas Maret, ISSN 1412-4092, e ISSN 2443-4183

left to stand at room temperature for 48 hours, during which it transformed into a gel. The resulting gel was dried in an oven at 80 °C for 3 hours, then calcined at 500 °C for 2 hours, yielding white TiO_2 powder.

Synthesis of TiO_2/Fe_2O_3 Composites

The TiO_2/Fe_2O_3 composite was synthesized via a simultaneous sol-gel method, following the procedure described by Khasawneh *et al.* (2020), with slight modifications. The $Fe(NO_3)_3 \cdot 9H_2O$ solution (0.0012 mol) was prepared by dissolving 0.5 g of $Fe(NO_3)_3 \cdot 9H_2O$ powder in 10 mL of distilled water. This solution was then added to a previously prepared TiO_2 sol while stirring at room temperature for 120 minutes to yield an Fe-TiO_2 sol. Subsequently, the Fe-TiO_2 sol was left to stand for 3 days until a gel formed, dried in an oven at 100 °C for 12 hours, and finally calcined at 500 °C for 2 hours to obtain the TiO_2/Fe_2O_3 composite as a reddish-white powder.

Synthesis of Graphene Oxide (GO) and Reduced Graphene Oxide (rGO)

Graphene oxide (GO) was synthesized using a modified Hummers' method (Lavelim *et al*., 2023). Graphite powder (2.5 g) was added to 57.5 mL of an H_2SO_4/H_3PO_4 mixture (9:1) and stirred continuously for 30 minutes until the temperature reached approximately 10 °C. Subsequently, 3 g of $KMnO_4$ powder was slowly added under constant stirring for 30 minutes, while maintaining the temperature below 20 °C. The suspension was heated to 40 – 50 °C and stirred for 40 minutes. Next, 125 mL of distilled water was gradually added while stirring, and the mixture was allowed to oxidize at room temperature for 30 minutes. Then, 30% hydrogen peroxide (2.5 mL) was added slowly while stirring for 30 minutes. The suspension was left to stand for 12 hours, filtered using Whatman filter paper, and washed with 100 mL of 1 M hydrochloric acid followed by demineralized water. The resulting GO solid was washed again with demineralized water until the pH shifted from 3.0 to 5. Finally, the solid was dried in an oven at 60 °C for 12 hours, yielding a dark brown GO powder.

The synthesis of reduced graphene oxide (rGO) was carried out based on our previous study (Hidayati *et al*., 2021). One gram of GO powder was dispersed in 25 mL of ethylene glycol and sonicated (20 kHz) for 2 hours. Then, 1 mL of hydrazine hydrate (N_2H_4) was added to the GO suspension, followed by 1 hour of sonication. The suspension was subsequently placed in a sealed autoclave and heated at 100 °C for 6 hours. The mixture was then centrifuged at 3500 rpm for 10 minutes to separate the solid product. Finally, the separated rGO solid was washed sequentially with deionized water and ethanol until the pH shifted to the range of 5.0 – 6.0. The solid was dried at 80 °C for 12 hours to obtain rGO powder (Hidayati *et al*., 2021).

Synthesis of TiO_2/Fe_2O_3/rGO Composites

The TiO_2/Fe_2O_3/rGOx composite was synthesized via a hydrothermal method following the procedure described by Utami *et al*. (2024), with slight modifications. Specifically, 0.015 g of rGO powder was mixed with 40 mL of demineralized water and 20 mL of ethanol, then sonicated (20 kHz) for 2 hours (Khavar *et al*.,2018). Subsequently, 1.5 g of the TiO_2/Fe_2O_3 composite was added to the rGO suspension and stirred for 2 hours until a homogeneous suspension was formed. Using the same conditions, the rGO content was varied at w/w ratios of 1%, 2%, and 3% relative to the TiO_2/Fe_2O_3 weight; the resulting TiO_2/Fe_2O_3/rGO composites (where x = 1, 2, or 3%) were designated as TF1, TF2, and TF3, respectively. The resulting suspension was transferred into the Teflon chamber of a 100 mL hydrothermal autoclave reactor and heated at 120 °C for 7 hours. Finally, the mixture was centrifuged at 3500 rpm for 10 minutes, washed with demineralized water, and dried in an oven at 60 °C for 7 hours to yield the TiO_2/Fe_2O_3/rGO composite.

Characterization

The obtained TiO_2/Fe_2O_3/rGO composite was characterized using several appropriate methods to evaluate its structural, optical, and surface properties. Crystalline phase structural characteristics were determined via X-Ray Diffraction (XRD; PW3040/60 PANalytical) analysis using Cu Kα1 (λ = 0.154 nm) radiation over a 20° – 80° range, with a step width of 0.02° and a scan speed of 2.00°/min. The diffractogram measurement data were used to calculate the phase, and the average crystallite size was determined using the Debye Scherrer equation as Equation 1 (Roopa *et al*., 2026).

$$D = \frac{K\lambda}{\beta \cos \theta} \quad (1)$$

where D is the particle size (nm), K is a value of 0.9, β (rad) is the full width at half maximum (FWHM), λ (0.154 nm) is the X-ray wavelength, and θ is the angle of incidence (rad).

Copyright © 2026, Universitas Sebelas Maret, ISSN 1412-4092, e ISSN 2443-4183

Information on surface functional groups and chemical bonds was obtained using a Fourier Transform Infrared (FTIR) spectrophotometer (Shimadzu IRPrestige-21), with spectra recorded over the 4000 – 400 cm^{-1} wavenumber range. The optical properties of the TiO_2/Fe_2O_3/rGO composite were examined using a UV-Vis Diffuse Reflectance Spectrophotometer (DRS UV-Vis; PerkinElmer LAMBDA 365) operating within the 200–800 nm wavelength range. The measured reflectance spectra were transformed into the Kubelka–Munk (KM) function as a function of photon energy (hν) to calculate the band gap (Eg). The band gap energy (Eg) of the investigated catalyst material was calculated based on the onset of the absorption edge using the formula presented in Equations 2 – 3 (Aritonang *et al.*, 2025).

$$F\,(R\infty) = \frac{K}{S} = + \frac{(1-R\infty)^2}{2R\infty} \quad (2)$$

$$(F(R\infty).hv)^{1/\gamma} = B(hv - Eg) \quad (3)$$

where h, v, Eg, and B represent Planck's constant, photon energy, band gap energy, and a constant, respectively. The factor γ depends on the nature of the electron transition and takes a value of 1/2 or 2 for direct and indirect band gap transitions, respectively.

Photocatalytic Activity Test

The photocatalytic activity of the synthesized TiO_2/Fe_2O_3/rGOx composite was evaluated for the degradation of tetracycline solution using the method of Mohammadi *et al.* (2023) with slight modifications. A total of 0.1 gram of TiO_2/Fe_2O_3/rGOx composite was added to a glass beaker, which had previously been filled with 100 mL of tetracycline solution with a concentration of 30 ppm. Prior to measurement, the pH was adjusted to 5.6 by adding 1 M HCl and 0.1 M NaOH solutions. Then the test solution was kept in a dark room for 30 minutes to reach adsorption-desorption equilibrium. Next, the test solution was placed in a photocatalysis reactor equipped with 6 LED lamps, each rated at 20 watts. At specific time intervals (0, 30, 60, 90, and 120 minutes), approximately 3.0 mL of the TC suspension was centrifuged at 4500 rpm for 30 minutes to separate the photocatalyst present in the solution.

To determine the photocatalytic degradation of TC, UV-Vis spectrophotometric analysis was performed using a Thermo Scientific Orion AquaMate 8100 at the maximum wavelength (λmax = 360 nm). The absorbance value (A) obtained from spectrophotometric measurement is subsequently analyzed using the Beer-Lambert equation (A = εbC), where A is the absorbance, ε is the molar absorptivity coefficient, b is the cuvette path length, and C is the concentration. Deviations in the preparation of the test solution can be considered negligible, as the curve's linearity yielded an R^2 value of 0.9981.

RESULTS AND DISCUSSION

The FTIR spectra of the Sargassum extract, TiO_2, and the TiO_2/Fe_2O_3 composite synthesized via the green method are presented in Figure 1. Based on the infrared spectra of the *Sargassum sp.* extract, several characteristic absorption bands corresponding to functional group stretching vibrations were identified; notably, an absorption at a wavenumber of approximately 3425 cm^{-1} indicates the presence of hydroxyl (O–H) groups derived from polysaccharide or phenolic compounds (Fakhouri, 2026; Khalafu *et al.*, 2017).

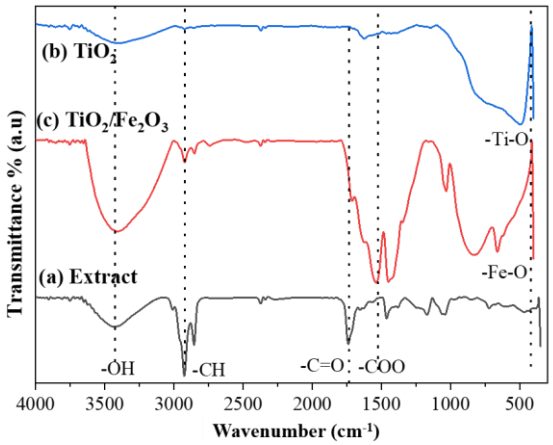


Figure 1. The FTIR spectra of (a) *Sargassum sp.* extract, (b) TiO_2, and (c) TiO_2/Fe_2O_3.

Copyright © 2026, Universitas Sebelas Maret , ISSN 1412-4092, e ISSN 2443-4183

In addition, an absorption band at wavenumber 2924 cm^{-1} from C–H vibrations was observed, followed by an absorption band with a weak intensity at 1462 cm^{-1} originating from single bonds between sp3 carbon atoms (C–C). The absorption position then identified the typical ester compound content in the extract, which was characterized by a carbonyl group band (C=O) with medium intensity at a wavenumber of 1739 cm^{-1} and a C–O ether group band with weak intensity at 1170 cm^{-1}. Apart from that, absorption bands were also identified at 1242 cm^{-1} and 1039 $cm^{-1,}$ which indicate the presence of C–O–C vibrations of fucoidan (sulfate polysaccharide) as a reducing and capping agent in nanoparticle synthesis (Hong *et al*., 2021; Khalafu *et al*., 2017; Li *et al*., 2021; Sobuj *et al*., 2024). The presence of oxygen-carrying functional groups can support the potential of Sargassum sp. extract as a natural reducing and stabilizing agent, forming a thin organic layer during nanoparticle synthesis (Aritonang *et al*., 2025; Fakhouri, 2026; Khalafu *et al*., 2017; Li *et al*., 2021). In addition to acting as a stabilizing and reducing agent in the synthesis of TiO_2 and TiO_2/Fe_2O_3 composites, the brown seaweed extract (*Sargassum sp.*) can also function as a chelating agent, as illustrated in Figures 1b and 1c. FTIR spectral analysis identifies the interaction between the asymmetric (ν_{as}) and symmetric (ν_s) stretching bands of the carboxylate group (COO^-) derived from the brown seaweed extract (*Sargassum sp.*) and titanium metal atoms to form the TiO_2/Fe_2O_3 composite (bridging bidentate mode) (Farkaš et al., 2020). These interaction modes illustrate how oxygen atoms from the carboxylate groups in the extract *Sargassum sp.* interact with metal ions, a process that contributes to the formation of more uniform and controlled particles (Farkaš *et al*., 2020).

The crystalline phases of the TiO_2/Fe_2O_3/rGO composite were identified using X-ray diffraction (XRD), as shown in Figure 2. The diffraction peak (100) is used in the Bragg equation to determine the distance (d) between graphene layers and is substituted into the Scherrer formula with a constant of 0.9 (Equation 1). Figure 2A shows the XRD patterns of rGO and TiO_2/Fe_2O_3/rGO composites with varying rGO content of 1% (TF1), 2% (TF2), and 3% (TF3). The XRD pattern in Figure 2A (a) shows the presence of a main diffraction peak typical of rGO material at $2\theta = 26.02^o$ and 42.15^o, which corresponds to the (100) and (002) crystal plane (Utami *et al*., 2024). Meanwhile, each XRD pattern in Figure 2A (b-d) shows diffraction peaks with strong intensity at (2θ) angles of 25.17^o (TF1), 25.26^o (TF2), and 25.14^o (TF3), all of which correspond to the with Miller index values (hkl) (101) plane of anatase phase TiO_2 based on JCPDS-ICDD standard data 03-065-5714 (Zajac *et al*., 2022). The rGO sample exhibits a broad diffraction peak at approximately $2\theta \approx 24°$, corresponding to the (100) plane of graphitic carbon, indicating partial reduction and the rearrangement of graphene oxide sheets, as shown in Figure 2.B (a) (Botsa, 2025). However, the typical diffraction peaks of rGO and α-Fe_2O_3 were not visible in the three XRD patterns of the TF1, TF2, and TF3 composites. The resulting diffraction peaks can indicate the successful synthesis of anatase TiO_2.

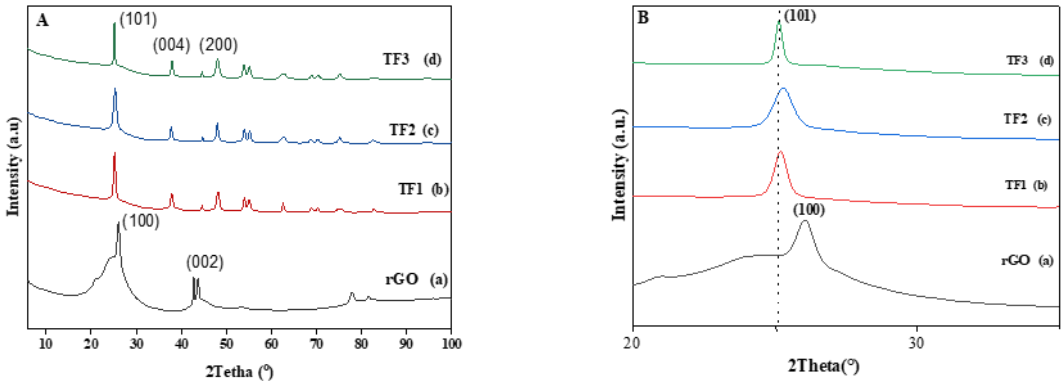


Figure 2. The XRD diffractograms presented in (A) full range 10 – 100° and (B) the emphasized range of 20 – 35° for the samples: (a) rGO, (b) TF1, (c) TF2, (d) TF3.

This is thought to be due to the overlap between the diffraction peaks of anatase TiO_2 (101) and those of rGO, as well as the low concentration of Fe_2O_3, resulting in a very small diffraction contribution (Zajac *et al*., 2022). However, for the (101) plane, a shift of the diffraction peak toward a lower 2θ angle was observed in the composite samples (Figure 2) (TF1 – TF3). This indicates a change in the lattice parameters of the anatase TiO_2 crystal structure at an angle of 25.37^o (Hossain and Ahmed, 2023). The results shown in Figure 2 demonstrate that the hydrothermal synthesis route effectively produces a ternary TiO_2/Fe_2O_3/rGO heterostructure, with the crystalline phases of both oxides well preserved and anchored to the GO matrix. The results shown in Figure 2

Copyright © 2026, Universitas Sebelas Maret
, ISSN 1412-4092, e ISSN 2443-4183

demonstrate that the combined green synthesis and hydrothermal method effectively produces a ternary TiO_2/Fe_2O_3/rGO heterostructure, with the crystalline phases of both oxides well preserved.

The functional groups of the synthesized materials were analyzed using the FTIR spectra shown in Figure 3. The FTIR spectra of TiO_2 and the TiO_2/Fe_2O_3 composite (Figure 3) synthesized via a green method using brown seaweed (*Sargassum sp.*) extract exhibit characteristic absorption peaks corresponding to Ti-O and Fe–O bands in the wavenumber regions of approximately 491 – 493 cm^{-1} and 721 cm^{-1} (Mohammadi *et al*., 2023; Utami *et al*., 2024). Additionally, absorption bands associated with the stretching and bending vibrations of water molecules (H_2O) are observed at 3417 – 3444 cm^{-1} and 1624 – 1626 cm^{-1} in both the TiO_2 and the TiO_2/Fe_2O_3 composite (Mohammadi *et al*., 2023).

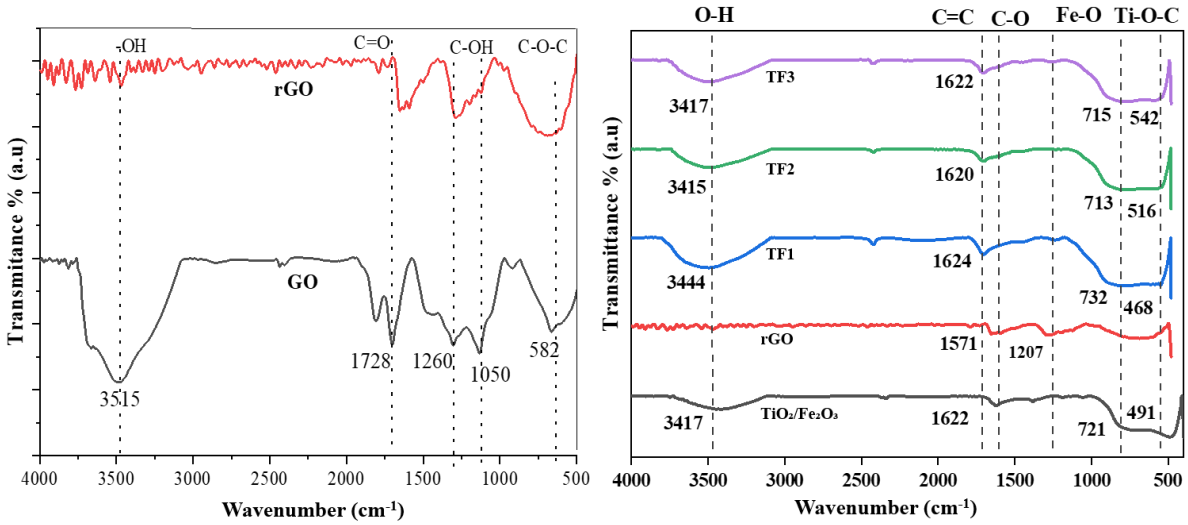


Figure 3. FTIR spectra of: (left) GO and rGO, (right) TiO_2/Fe_2O_3, rGO and TiO_2/Fe_2O_3/rGO composites: TF1, TF2, and TF3.

The functional group analysis was subsequently performed on the Graphene Oxide (GO) material, with the resulting spectra shown in Figure 3. The FTIR spectral analysis was conducted to confirm the intercalation of oxygen-containing groups into the GO interlayer spaces following graphite oxidation. As shown in Figure 3, a broad, high-intensity absorption peak appears at a wavenumber of approximately 3415 cm^{-1} due to stretching vibrations, indicating the presence of hydroxyl (O–H) groups in the GO. Additional absorption bands appear at 1728 cm^{-1}, indicating carbonyl (C=O) groups, and in the 1260 – 1050 cm^{-1} range, indicating ether (C–O) groups. Furthermore, a distinct absorption peak corresponding to epoxy (C–O–C) groups is observed at 582 cm^{-1}, possibly present in the GO layer structure (Utami *et al*., 2024). Based on the identification of these oxygen-containing functional groups (hydroxyl, carbonyl, and epoxy), it is confirmed that the GO material was successfully synthesized via the graphite oxidation reaction (Magro *et al*., 2025). Functional group analysis was also performed on the reduced Graphene Oxide (rGO) material obtained from the subsequent reduction of the GO material. The rGO FTIR spectra in Figure 3 reveal several peaks with reduced absorption intensity after the reduction process. For instance, the peak associated with hydroxyl (O–H) groups on the rGO surface at 3387 cm^{-1} shows reduced intensity. The other absorption peaks, such as the carbonyl group (C=O) at 1728 cm^{-1}, the ether group (C–O) in the 1260 – 1050 cm^{-1} range, and the epoxy group (C–O–C) at 582 cm^{-1}, also exhibited decreased absorption intensity compared to the functional groups detected in the GO FTIR spectra (Figure 3). Furthermore, functional group analysis of the rGO material revealed an increase in absorption intensity at 1571 cm^{-1}, indicating C=C bond stretching vibrations in the aromatic structure following the reduction process (Utami *et al*., 2024). These results confirm the successful reduction or partial removal of oxygen-containing groups (hydroxyl, carbonyl, and epoxy) from the GO layer structure using hydrazine monohydrate as the reducing agent, although a small amount of oxygen-containing groups remained incompletely reduced (Kaftelen-Odabaşi, 2024; Xu *et al*., 2014). Subsequent FTIR spectra showed an increase in absorption peak intensity following the incorporation of rGO into the TiO_2/Fe_2O_3 composite via the hydrothermal method, with rGO loadings of 1%, 2%, and 3% by mass (w/w) (Sari *et al*., 2019). Based on the FTIR spectra in Figure 3, several detected absorption peaks corresponding to the stretching vibrations of hydroxyl (O–H) groups and carbon-carbon double bonds (C=C) exhibited increased

Copyright © 2026, Universitas Sebelas Maret, ISSN 1412-4092, e ISSN 2443-4183

intensity in the TiO_2/Fe_2O_3 /rGO composites (1%, 2%, 3%) compared to the TiO_2/Fe_2O_3 composite (without rGO). The increased absorption intensity of the hydroxyl (O–H) group may be attributed to the formation of hydrogen bonds between oxygen-containing groups on the incompletely reduced rGO and hydroxyl (O–H) groups on the composite surface, as well as the inherent hygroscopic nature of rGO. Furthermore, the increased absorption intensity of the C=C bond in the composite may result from the contribution of conjugated C=C bonds within the rGO aromatic structure integrated into the TiO_2/Fe_2O_3 matrix. In addition to increasing absorption peak intensity, the incorporation of rGO can also lead to a decrease in intensity and peak broadening in the resulting TiO_2/Fe_2O_3 composite due to the formation of Ti–O–C bonds (Hidayati *et al*., 2021; Sari *et al*., 2019; Utami *et al*., 2024). These results indicate the successful formation of the TiO_2/Fe_2O_3/rGO composite.

Based on measurements using the UV-Vis diffuse reflectance spectrophotometry method within the 200 – 700 nm wavelength range and subsequent analysis via the Kubelka-Munk equations (Equations 2 and 3) by plotting $(\alpha hv)^{1/2}$ against hν, the band gap value was determined, as shown in Figure 4. Figure 4 reveals that the green-synthesized TiO_2 has a band gap of 3.26 eV. Combining TiO_2 with Fe_2O_3 resulted in a reduction of the band gap to 2.97 eV.

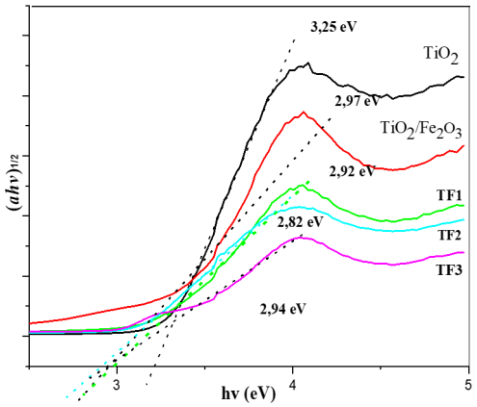


Figure 4. Curve $(ahv)^{1/2}$ versus hv (eV).

According to Khasawneh *et al.* (2020), the reduction in band gap energy is attributed to the influence of Fe_2O_3 formed on the TiO_2 surface; this induces interfacial interactions that lead to crystal defects in the TiO_2, specifically the transition from Ti–O–Ti to Ti–O–Fe bonds, thereby altering the electronic structure of the TiO_2 and creating a heterojunction structure that is crucial for inhibiting electron-hole pair recombination at the TiO_2 surface. The addition of rGO to form the TiO_2/Fe_2O_3/rGO composite resulted in a reduction of the band gap, albeit a slight one, yielding values of 2.92, 2.85, and 2.94 eV, respectively. Based on these band gap values, the TiO_2/Fe_2O_3/rGO composite is expected to absorb energy ranging from the UV to the visible-light region. Notably, the TiO_2/Fe_2O_3/rGO composite exhibited enhanced, broader absorption across both the UV and visible regions compared to its individual components, indicating effective interfacial charge transfer and synergistic light-harvesting capabilities. These results demonstrate that incorporating rGO into the TiO_2/Fe_2O_3 matrix significantly improves optical response, a crucial factor for photocatalytic activity.

Photocatalytic Degradation of Tetracycline

The photocatalytic activity of the synthesized TiO_2/Fe_2O_3/rGO composite under visible light irradiation (λ>415 nm) was evaluated by decreasing the TC concentration in the test solution. The test solution was prepared by dissolving tetracycline in demineralized water to obtain a model concentration of 30 ppm. TC concentration measurements were carried out using UV-Visible spectrophotometry, with absorbance (A) recorded at the maximum wavelength of TC (λmax) = 360 nm (Mohammadi *et al*., 2023). The photocatalytic degradation of TC was monitored using a non-exhaustive method, in which TC concentration measurements were limited to 120 minutes. The remaining concentration (C) in the test solution is determined by converting A using the Lambert-Beer equation. The percentage (%) of degraded TC was determined using Equation 4 (Mohammadi *et al*., 2023).

$$\%\ \text{degraded} = \frac{(Co - Ct)}{Co} \text{x} + 100\% \qquad (4)$$

Here, C_o and C_t represent the initial and final TC concentrations (ppm), respectively. The percentage of TC degradation was calculated from the measured absorbance values using Equation 4. This value indicates the

Copyright © 2026, Universitas Sebelas Maret, ISSN 1412-4092, e ISSN 2443-4183

efficiency of photocatalytic TC removal from the test solution. Subsequently, the percentage of TC degradation for each sample can be determined. The percentage (%) of TC degradation via photocatalysis under visible light irradiation is shown in Figure 5.

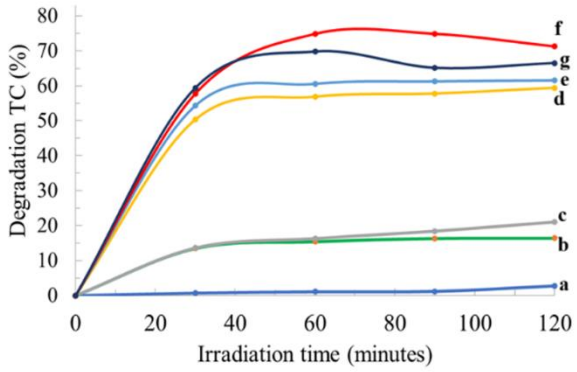


Figure 5. The percentage degradation of TC versus irradiation time curve (%D) by the process of (a) visible-light photolysis, (b) adsorption TF2; Photocatalysis using of the (c) TiO_2, (d) TiO_2 /Fe_2O_3, (e) TF1, (f) TF3, and (g) TF2.

Figure 5 shows the percentage of TC degraded by three processes: visible-light photolysis, adsorption by the TF2 catalyst (dark state), and photocatalysis (catalyst and light). It can be seen that the photolysis process under visible light degrades TC by 1.8%, and the adsorption process by TF2 by 11.6%. Photocatalysis using TiO_2 degraded only 12.4% of TC. As TiO_2 has a band gap of 3.26 eV, it can only be activated when absorbing UV light. In this study, an insignificant difference was observed between the TiO_2 adsorption and photocatalysis processes. It is possible that the LED lamp used as a source of visible light still contains a small amount of UV light. TiO_2/Fe_2O_3 photocatalysis shows good activity under visible-light irradiation, degrading TC by 54%. The combination of Fe_2O_3 with the semiconductor TiO_2 as overlapping 2p orbitals causes a change in the band gap from 3.26 eV to a narrower 2.97 eV (Khasawneh *et al*., 2020; Aritonang *et al*., 2021). The incorporation of rGO into the TiO_2/Fe_2O_3 matrix (yielding samples TF1, TF2, and TF3) enhanced the photocatalytic activity for TC degradation. This improved degradation efficiency is attributed to the interaction between TiO_2, Fe_2O_3, and rGO, which forms a heterojunction structure (Botsa, 2025). The TiO_2/Fe_2O_3 interface facilitates charge transfer between the semiconductors, thereby minimizing the recombination of active charge carriers (Jo and Selvam, 2015). TF2 exhibited the highest activity, achieving 72% TC degradation, whereas TF1 and TF3 achieved 58% and 63% degradation, respectively. The addition of rGO at a 3% ratio likely led to partial coverage of the catalyst's active surface, thereby limiting visible-light penetration. Based on these results, it can be concluded that the optimum rGO ratio is 2%, yielding a TC degradation efficiency of 72%.

CONCLUSION

The TiO_2/Fe_2O_3 heterojunction composite was successfully synthesized via a combined green synthesis method that used Sargassum extract and a hydrothermal process. Incorporating Fe_2O_3 into the TiO_2 matrix reduced the band gap from 3.26 eV to 2.97 eV, enabling visible-light activation of the photocatalyst to degrade 54% of TC (at a concentration of 30 ppm) over 120 minutes. The addition of rGO to the TiO_2/Fe_2O_3 composite matrix at an optimal rGO:(TiO_2/Fe_2O_3) weight ratio of 2%, forming the TiO_2/Fe_2O_3/rGO (TF3) composite, resulted in a TC degradation efficiency of 72%. This enhanced photocatalytic activity for TC degradation stems from the synergistic contribution of the TiO_2/Fe_2O_3 heterojunction composite and rGO, which promotes the separation of active charge pairs.

CONFLICT OF INTEREST

There are no conflicts of interest in this article.

AUTHOR CONTRIBUTION

ABA: Conceptualization, Investigation, Methodology, and Manuscript Drafting; HTMR: Project Administrator and Tools Software; MAW: Data Analysis, Validation, and Manuscript Review; WW: Supervision, Manuscript Review and Editing.

Copyright © 2026, Universitas Sebelas Maret, ISSN 1412-4092, e ISSN 2443-4183

ACKNOWLEDGMENT

This work was supported by DIPA Tanjungpura University, Grant 139.03.2.693380/2025 dated December 2, 2024 Contract No.: 2312/UN22.8/PT.01.05/2025.

DECLARATION OF GENERATION AI

No declaration of generative AI use was provided.

REFERENCES

Aritonang, A.B., Putri, R.A., Sisca, V., Madiabu, M.J., and Khoiriah, K., 2025. Photocatalytic Degradation of Acid Yellow 25 Using Nanoparticle TiO_2 Mediated Petai Pod Extract. *Baghdad Science Journal*, 22, 1851–1862. https://doi.org/10.21123/2411-7986.4960.

Aritonang, A.B., Krisnandi, Y.K., and Gunlazuardi, J., 2018. Modification of TiO_2 Nanotube Arrays with N Doping and Ag Decorating for Enhanced Visible Light Photoelectrocatalytic Degradation of Methylene Blue. *International Journal on Advanced Science Engineering Information Technology*, 8, 234–24. https://doi.org/10.18517/ijaseit.8.1.2342.

Aritonang, A.B., Parwanty, P., Wibowo, M.S., Ardiningsih, P., and Adhitiyawarman, A., 2022. Sintesis TiO_2-rGO dengan Pereduksi Alumunium untuk Fotokatalisis Degradasi Metilen Biru dibawah Irradiasi Sinar Tampak, *Equilibrium Journal of Chemical Engineering*, 6, 150–156. https://doi.org/10.20961/equilibrium.v6i2.65518.

Aritonang, A.B., Pratiwi E., Warsidah., Nurdiansyah S.I, and Risko., 2021. Fe-doped TiO_2/Kaolinite as an Antibacterial Photocatalyst under Visible Light Irradiation. *Bulletin of Chemical Reaction Engineering & Catalysis*, 16, 293–301. https://doi.org/10.9767/bcrec.16.2.10325.293-301.

Botsa, M.B., 2025. Reduced Graphene Oxide Assisted TiO_2 Fe_2O_3 Ternary Nanocomposite for Efficient Visible Light Driven Photocatalysis of Nitrobenzene and Dye Pollutants. *Advanced Composites and Hybrid Materials*, 8, 384–399. https://doi.org/10.1007/s42114-025-01431-w.

Cao, Y., Yang, W., Zhang, W., Liu, G., and Yue, P., 2004. Improved Photocatalytic Activity of Sn^{4+} Doped TiO_2 Nanoparticulate Films Prepared by Plasma-Enhanced Chemical Vapor Deposition. *New Journal of Chemistry*, 28, 218–222. https://doi.org/10.1039/b306845e.

Chang, C., Rad, S., Gan, L., Li, Z., Dai, J., and Shahab, A., 2023. Review of The Sol-Gel Method in Preparing Nano TiO2 for Advanced Oxidation Process. *Nanotechnology Reviews*, 12, 1–23. https://doi.org/10.1515/ntrev-2023-0150.

Elmund, G.K., Mormson, S.M., Grant, D.W., and Nevlns, S.M.P., 1971. Role of Excreted ChlorTetracycline in Modifying the Decomposition Process in Feedlot Waste. *Bulletin of Environmental Contamination & Toxicology*, 6, 129–132.

Fakhouri, A.S., 2026. Biotechnological Potential of Sargassum Ilicifolium Seaweed: A Proximate Composition of Antibacterial, Antioxidant, and Hypoglycemic Bioactive Compounds. *BioResources*, 21, 3872–3893. https://doi.org/10.15376/biores.21.2.3872-3893

Farkaš, B., Terranova, U., and de Leeuw, N.H., 2019. Binding Modes of Carboxylic Acids on Cobalt Nanoparticles. *Royal Society of Chemistry*, 22, 985–996. https://doi.org/10.1039/c9cp04485j

Hidayati, U.F., Aritonang, A.B., and Destiarti, L., 2021. TiO_2-rGO Composite for Photocatalytic Decolorization of Methylene Blue Under the Visible Light Illumination. *Berkala Sainstek*, 9, 167–173. https://doi.org/10.19184/bst.v9i4.27602.

Hong, T., Yin, J.Y., Nie, S.P., and Xie, M.Y., 2021. Applications of Infrared Spectroscopy in Polysaccharide Structural Analysis: Progress, Challenge and Perspective. *Food Chemistry*, 12, 100168. https://doi.org/10.1016/j.fochx.2021.100168.

Hossain, M.S., and Ahmed, S., 2023. Easy and Green Synthesis of TiO_2 (Anatase and Rutile): Estimation of Crystallite Size Using Scherrer Equation, Williamson-Hall Plot, Monshi-Scherrer Model, Size-Strain Plot, Halder- Wagner Model. *Results in Materials*, 20, 100492. https://doi.org/10.1016/j.rinma.2023.100492.

Jo, W., and Selvam, N.C.S., 2015. Synthesis of GO Supported Fe_2O_3–TiO_2 Nanocomposites for Enhanced Visible-Light Photocatalytic Applications. *Dalton Transactions*, 44, 16024–16035 https://doi.org/10.1039/c5dt02983j.

Juma, A.O., Acik, I.O., Mikli, V., Mere, A., and Krunks, M., 2015. Effect of Solution Composition on Anatase to Rutile Transformation of Sprayed TiO_2 Thin Films. *Thin Solid Films*, 594, 1–6. https://doi.org/10.1016/j.tsf.2015.03.036.

Kaftelen-Odabaşi, H., 2024. Evaluation of Morphological, Structural, Thermal, Electrical, and Chemical Composition Properties of Graphene Oxide, and Reduced Graphene Oxide Obtained by Sequential Reduction Methods. *Carbon Trends*, 17, 1–10. https://doi.org/10.1016/j.cartre.2024.100429.

Copyright © 2026, Universitas Sebelas Maret, ISSN 1412-4092, e ISSN 2443-4183

Khalafu, S.H.S., Wan Aida, W.M., Lim, S.J., and Maskat, M.Y., 2017. Effects of Deodorisation Methods on Volatile Compounds, Chemical Properties and Antioxidant Activities of Fucoidan Isolated from Brown Seaweed (*Sargassum sp*.). *Algal Research*, 25, 507–515. https://doi.org/10.1016/j.algal.2017.06.018.

Khasawneh, O.F.S., and Palaniandy, P., 2020. Removal of Organic Pollutants from Water by Fe2O3/TiO2 Based Photocatalytic Degradation : A Review. *Environmental Technology & Innovation*, 30, 1–20. https://doi.org/10.1016/j.eti.2020.101230.

Khavar, C.A.H., Moussavi, G., and Mahjoub, A.R. 2018. The preparation of TiO2 @rGO Nanocomposite efficiently Activated with UVA/LED and H_2O_2 for High Rate Oxidation Of Acetaminophen: Catalyst Characterization and Acetaminophen Degradation and Mineralization. *Applied Surface Science*, 440, 963–973. https://doi.org/10.1016/j.apsusc.2018.01.238.

Lavelim, B., Destiarti, L., Adhitiyawarman, A., and Sasri, R., 2023. Synthesis of Reduced Graphene Oxide-Bentonite Composite and Its Application as a Lead (II) Ion Adsorbent. *Indonesian Journal of Chemistry*, 23, 1–11. https://doi.org/10.22146/ijc.67993.

Li, Y., Zheng, Y., Zhang, Y., Yang, Y., Wang, P., Imre, B., Wong, A.C.Y., Hsieh, Y.S.Y., and Wang, D., 2021. Brown Algae Carbohydrates: Structures, Pharmaceutical Properties, and Research Challenges. *Marine Drug*s, 19, 1–21. https://doi.org/10.3390/md19110620.

Magro, M.R., Vella, D.A., and Cassar, G., 2025. Synthesis of Graphene Oxide: A Refined Approach. *Carbon Trends*, 20, 100509. https://doi.org/10.1016/j.cartre.2025.100509.

Mei, Q., Zhang, F., Wang, N., Yang, Y., Wu, R., and Wang, W., 2019. TiO_2/Fe_2O_3 Heterostructures with Enhanced Photocatalytic Reduction of Cr(VI) under Visible Light Irradiation. *Royal Society of Chemistry*, 9, 22764–22771. https://doi.org/10.1039/c9ra03531a.

Mohamed, H.H., Alomair, N.A., Akhtar, S., and Youssef, T.E., 2019. Eco-Friendly Synthesized α-Fe_2O_3/TiO_2 Heterojunction with Enhanced Visible Light Photocatalytic Activity. *Journal of Photochemistry and Photobiology A: Chemistry*, 382, 1–12. https://doi.org/10.1016/j.jphotochem.2019.111951.

Mohammadi, M., Sabbaghi, S., Binazadeh, M., Ghaedi, S., and Rajabi, H., 2023. Type-1 α-Fe_2O_3/TiO_2 Photocatalytic Degradation of Tetracycline from Wastewater Using CCD-Based RSM Optimization. *Chemosphere*, 336, 1–13. https://doi.org/10.1016/j.chemosphere.2023.139311.

Padmanabhan, N.T., Nishanth, T., Louis, J., Mathew, D.T., Ganguly, P., John, H., and Pillai, S.C., 2021. Graphene Coupled TiO_2 Photocatalysts for Environmental Applications: A review. *Chemosphere*, 271, 129506–129539. https://doi.org/10.1016/j.chemosphere.2020.129506.

Palanisamy, B., Babu, C.M., Sundaravel, B., Anandan, S., and Murugesan, V., 2013. Sol–Gel Synthesis of Mesoporous Mixed Fe_2O_3/TiO_2 Photocatalyst : Application for Degradation of 4-Chlorophenol. *Journal of Hazardous Materials*, 252–253, 233–242. https://doi.org/10.1016/j.jhazmat.2013.02.060.

Prasad, G., Tamang, S., Jha, S., Bhattacharyya, N.K., and Biswas, J., 2025. A Theoretical Insight into Graphene-Based Materials: A DFT Study. Results in Surfaces and Interfaces, 18, 100463. https://doi.org/10.1016/j.rsurfi.2025.100463.

Rashid, M.M., Simončič, B., Zorc, M., Fink, R., Čelan Korošin, N., Šuligoj, A., Kovač, J., Jerman, I., and Tomšič, B., 2025. Synthesis of a New Amino/Phosphate-Modified TiO_2/rGO Hybrid Nanocomposite for Sustainable Textile Functionalization. *Journal of Environmental Chemical Engineering*, 13, 1–19. https://doi.org/10.1016/j.jece.2025.116555.

Rathi, V.H., Rejo, A., and Jayakumar, K., 2023. Applied Surface Science Advances Green Synthesis of Ag/CuO and Ag/TiO_2 Nanoparticles for Enhanced Photocatalytic Dye Degradation, Antibacterial, and Antifungal Properties. *Applied Surface Science Advances*, 18, 1–13. https://doi.org/10.1016/j.apsadv.2023.100476.

Roopa, M.C., Kallimani, S., Thirumala, S., and Mylarappa, M., 2026. Synthesis and Development of rGO/ZnO Composite for Photocatalytic Studies, *Next Materials*, 12, 102217. https://doi.org/10.1016/j.nxmate.2026.102217.

Sari, U.R.K., Wahyuningsih, S., and Ramelan, A., 2019. Preparation of Fe_2O_3-TiO_2/GO Composites as a Visible Light Oxidation Photocatalyst Material. *IOP Conference Series: Materials Science and Engineering*, 578, 1–8. https://doi.org/10.1088/1757-899X/578/1/012042.

Septiyanti, M., Liana, L., Sutriningsih, S., Kumayanjati, B., and Meliana, Y., 2019. Formulation and Evaluation of Serum from Red, Brown and Green Algae Extract for Anti- Aging Base Material Formulation and Evaluation of Serum from Red, Brown and Green Algae Extract for Anti-Aging Base Material. *AIP Conference Proceedings*, 2175, 1–12.

Silerio-Vázquez, F. de J., González-Burciaga, L.A., Antileo, C., Núñez-Núñez, C.M., and Proal-Nájera, J.B., 2024. Photocatalytic Degradation of Antibiotics in Water via TiO_2-x: Research Needs for Technological Advancements. *Journal of Hazardous Materials Advances*, 16, 1–20. https://doi.org/10.1016/j.hazadv.2024.100506.

Copyright © 2026, Universitas Sebelas Maret , ISSN 1412-4092, e ISSN 2443-4183

Sobuj, M.K.A., Shemul, M.S., Islam, M.S., Islam, M.A., Mely, S.S., Ayon, M.H., Pranto, S.M., Alam, M.S., Bhuiyan, M.S., and Rafiquzzaman, S.M., 2024. Qualitative and Quantitative Phytochemical Analysis of Brown Seaweed Sargassum Polycystum Collected from Bangladesh with Its Antioxidant Activity Determination. *Food Chemistry Advances*, 4, 1–9. https://doi.org/10.1016/j.focha.2023.100565.

Utami, M., Yenn, T.W., Alam, M.W., Ravindran, B., Husniati, Purnama, I., Salmahaminati, Hidayat, H., Dhetaya, F.N., and Salsabilla, S.N., 2024. Efficient Photocatalytic Bactericidal Performance of Green-Synthesised TiO_2/Reduced Graphene Oxide Using Banana Peel Extracts. *Heliyon*, 10, 1–20. https://doi.org/10.1016/j.heliyon.2024.e26636.

Xu, C., Yuan, R. S., and Wang, X., 2014. Selective Reduction of Graphene Oxide. *New Carbon Materials*, 29, 61–66. https://doi.org/10.1016/S1872-5805(14)60126-8.

Xu, L., Zhang, H., Xiong, P., Zhu, Q., Liao, C., and Jiang, G., 2021. Occurrence, Fate, and Risk Assessment of Typical Tetracycline Antibiotics in the Aquatic Environment: A Review. *Science of the Total Environment*, 753, 1–17. https://doi.org/10.1016/j.scitotenv.2020.141975.

Yang, H., 2021. Short Review A Short Review on Heterojunction Photocatalysts: Carrier Transfer Behavior and Photocatalytic Mechanisms. *Materials Research Bulletin*, 142, 1–9. https://doi.org/10.1016/j.materresbull.2021.111406.

Zajac, A.T., Synowiec, M., Zakrzewska, K., Zazakowny, K., Kowalski, K., Dziedzic, A., and Radecka, M., 2022. Scavenger-Supported Photocatalytic Evidence of an Extended Type I Electronic Structure of the Fe_2O_3@TiO_2 Interface. *Applied Materials & Interfaces*, 14, 38255–38269. https://doi.org/10.1021/acsami.2c06404.

Zhang, J., Zhou, P., Liu, J., and Yu, J., 2014. New Understanding of the Difference of Photocatalytic Activity among Anatase, Rutile and Brookite TiO_2. *Physical Chemistry Chemical Physics*, 16, 20382–20386. https://doi.org/10.1039/C4CP02201G.

Zheng, R., Yang, D., Chen, Y., Bian, Z., and Li, H., 2023. Fe_2O_3/TiO_2/Reduced Graphene Oxide-Driven Recycled Visible-Photocatalytic Fenton Reactions to Mineralize Organic Pollutants in a Wide PH Range. *Journal of Environmental Sciences*, 134, 11–20. https://doi.org/10.1016/j.jes.2022.01.042.

Copyright © 2026, Universitas Sebelas Maret, ISSN 1412-4092, e ISSN 2443-4183